Chiral Boron Cluster

DOI: 10.1002/anie.201402488

$[B_{30}]^-$: A Quasiplanar Chiral Boron Cluster**

Wei-Li Li, Ya-Fan Zhao, Han-Shi Hu, Jun Li, and Lai-Sheng Wang**

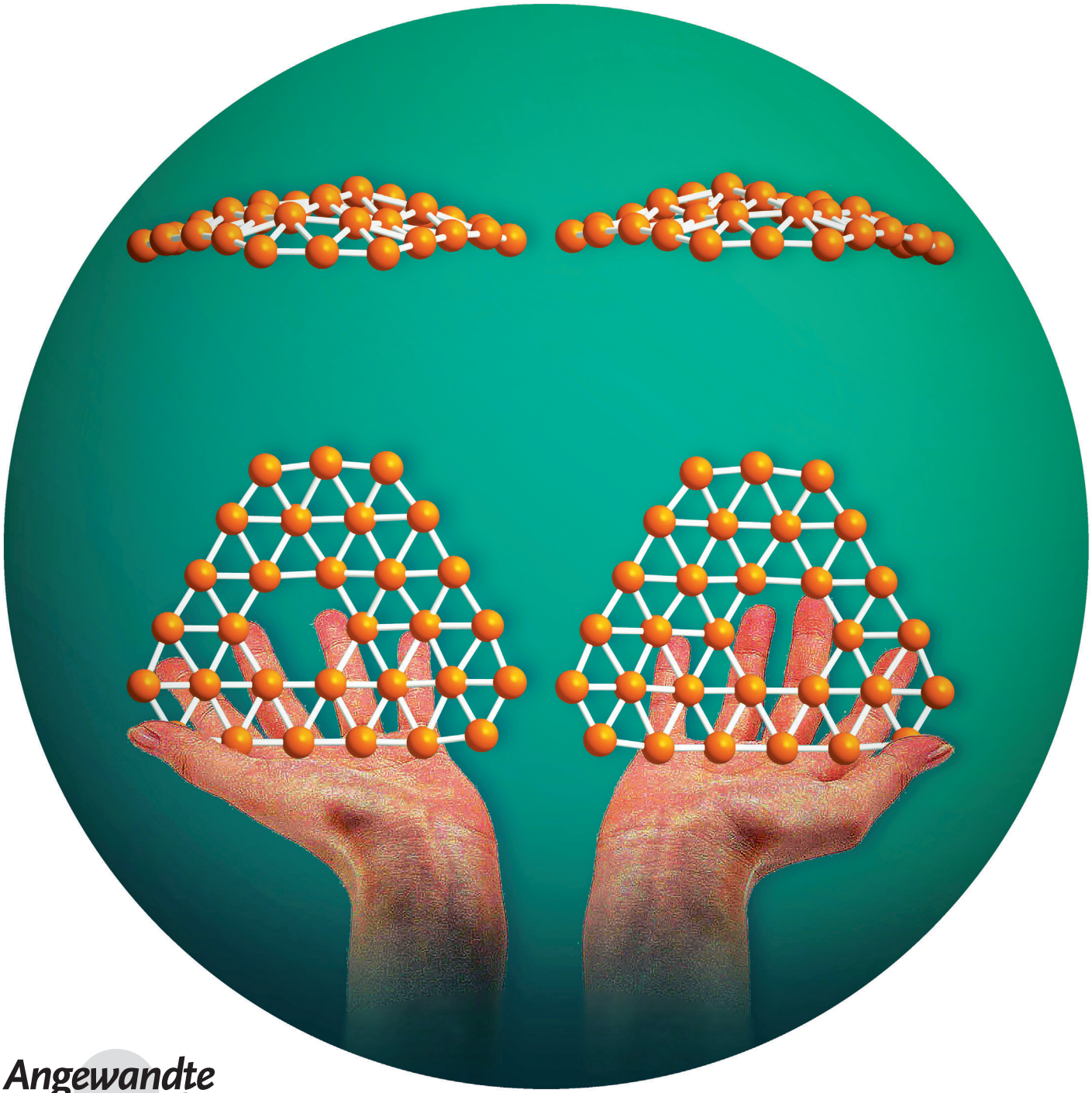

Abstract: *Chirality is vital in chemistry. Its importance in atomic clusters has been recognized since the discovery of the first chiral fullerene, the D_2 symmetric C_{76}.[1] A number of gold clusters have been found to be chiral,[2] raising the possibility to use them as asymmetric catalysts. The discovery of clusters with enantiomeric structures is essential to design new chiral materials with tailored chemical and physical properties.[3] Herein we report the first inherently chiral boron cluster of $[B_{30}]^-$ in a joint photoelectron spectroscopy and theoretical study. The most stable structure of $[B_{30}]^-$ is found to be quasiplanar with a hexagonal hole. Interestingly, a pair of enantiomers arising from different positions of the hexagonal hole are found to be degenerate in our global minimum searches and both should co-exist experimentally because they have identical electronic structures and give rise to identical simulated photoelectron spectra.*

Boron can form strong covalent bond with itself and almost all other elements in the periodic table. Because of its electron deficiency, bulk boron has unusual polymorphism built from three-dimensional (3D) cages.[4,5] However, joint experimental and quantum chemistry studies over the past decade have shown that the anionic boron clusters of up to 24 atoms are planar or quasiplanar, consisting of a peripheral ring characterized by two-center–two-electron (2c–2e) bonds and inner atoms that interact with the peripheral ring through delocalized bonds.[6–15] The σ- and π-electron delocalization in boron clusters gives rise to the concept of aromaticity in these species and rationalizes the stability of the planar or quasiplanar structures.

There have also been computational efforts exploring 2D boron nanostructures.[16–21] It was shown that boron is unable to form stable large nanosheets with honeycomb-like structures owing to its electron deficiency.[21] Instead, quasi-2D buckled triangular lattices appear to be more stable. Interestingly, hexagonal holes have been shown to be important to yield highly stable and truly planar atom-thin boron layers with a variety of hole densities (η).[22–26] Very recently, we have found that the $[B_{36}]$ cluster is a quasiplanar cluster with hexagonal symmetry and a perfect hexagonal hole in its center, providing the first experimental evidence that the 2D atom-thin boron layer with hexagonal holes is viable.[27] A name "borophene" was coined to designate the putative 2D boron sheet in analogy to graphene.[27] Tetragonal and pentagonal holes have been observed in smaller boron clusters, and $[B_{36}]$ and $[B_{36}]^-$ represent the first boron clusters to feature an interior hexagonal hole. It is expected that hexagonal holes should be a defining feature for large planar boron clusters. An interesting question is: what is the smallest boron cluster for an interior hexagonal hole to appear?

Herein we present a joint photoelectron spectroscopy (PES) and theoretical study of $[B_{30}]^-$, which is found not only to feature a hexagonal hole but also to have a unique chiral structure. A pair of enantiomers characterized by different positions of the hexagonal hole on the quasi-2D molecular plane is found to be the global-minimum structures of $[B_{30}]^-$, even though neutral $[B_{30}]$ is found to have a bowl-shaped global minimum with a pentagonal hole, in agreement with a recent computational study.[28] The chiral $[B_{30}]^-$ cluster can be viewed as removing six atoms from the edge of the hexagonal $[B_{36}]^-$, followed by a slight structural rearrangement.

The $[B_{30}]^-$ cluster was produced by a laser vaporization cluster source and probed by PES (see the Experimental Section for details). Figure 1a displays the PES spectrum of $[B_{30}]^-$ at 193 nm, where the observed spectral bands are labeled with letters (X, A, B …). The spectrum shows four well-defined bands (X, A, B, C) in the low binding energy region and more bands (D, E, F) in the high binding energy region, which are only tentatively labeled because of the poorer signal-to-noise ratios. The vertical detachment energy (VDE) of band X is measured to be 3.69(7) eV. The relatively sharp X band suggests there are probably only small geometry changes of the cluster upon electron detachment to neutral $[B_{30}]$. Since no vibrational structure is resolved, the

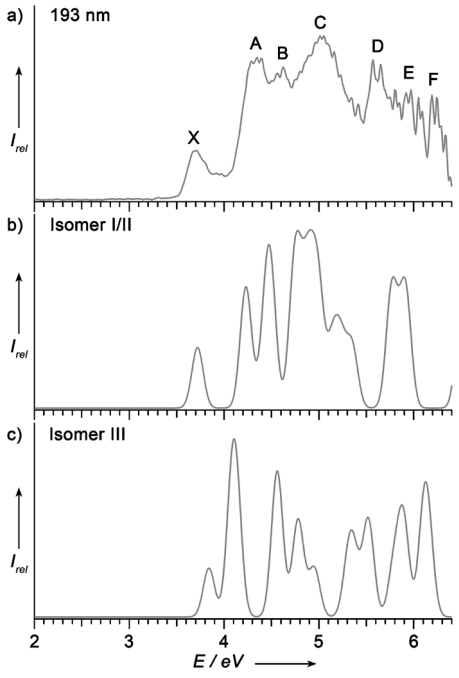

Figure 1. a) Photoelectron spectrum of $[B_{30}]^-$ at 193 nm; Simulated spectrum of b) isomer I and c) isomer III at TD-PBE0/6-311+G(2df).

[*] W. L. Li, Prof. Dr. L. S. Wang
Department of Chemistry, Brown University
Providence, RI 02912 (USA)
E-mail: Lai-Sheng_Wang@brown.edu
Dr. Y. F. Zhao, Dr. H. S. Hu, Prof. Dr. J. Li
Department of Chemistry & Key Laboratory of Organic Optoelectronics and Molecular Engineering of Ministry of Education
Tsinghua University, Beijing, 100084 (China)
E-mail: junli@tsinghua.edu.cn

[**] This work was supported by the U.S. National Science Foundation (CHE-1263745 to L.S.W) and NKBRSF (2011CB932401) and NSFC (21221062, 91026003) of China. The calculations were performed using the Supercomputer Center of the Computer Network Information Center, Chinese Academy of Sciences and the Shanghai Supercomputing Center.

Supporting information for this article is available on the WWW under http://dx.doi.org/10.1002/anie.201402488.

adiabatic detachment energy (ADE) is measured by drawing a straight line along the leading edge of band X and then adding the spectral resolution to the intersection with the binding energy axis. The ADE so determined is 3.59(7) eV. Following a gap of about 0.65 eV, three intense and broad bands, A, B, and C are observed with VDEs of 4.34(5), 4.61(5), and 5.03(8) eV, respectively. Band C is particularly broad, which must contain multiple detachment transitions, and the VDE is only a reference for the sake of discussion. The VDEs for bands D, E, and F are tentatively measured and all VDEs are given in Table 1, where they are compared with theoretical data (see below). The large X–A gap suggests that neutral $[B_{30}]$ should be a closed-shell species and the X–A separation is an approximate measure of the gap between the highest occupied (HOMO) and lowest unoccupied (LUMO) molecular orbitals of $[B_{30}]$. The non-zero intensity in the gap region between bands X and A may be due to a weakly populated low-lying isomer.

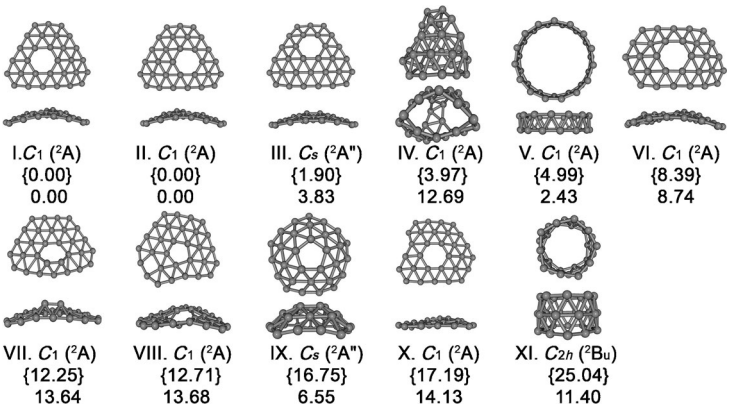

Figure 2. The global minimum and low-lying isomers (I–XI) of $[B_{30}]^-$. The relative energies are given in kcal mol^{-1} at LPNO-CCSD (in curly brackets) and PBE0 levels of theory. The relative energies at PBE0 level are corrected by zero-point energies (ZPE).

To determine the global minimum of $[B_{30}]^-$, we searched more than 3600 isomeric forms using the TGMin code (see the Experimental Section for details).[29] Figure 2 displays the structures, symmetries and electronic states of the lowest 11 isomers at the PBE0[30–32] and LPNO-CCSD[33,34] levels of theory. All the other isomers within 20 kcal mol^{-1} at PBE0 level are shown in Figure S1 of the Supporting Information. Interestingly, the global minima of $[B_{30}]^-$ are found to consist of two degenerate quasiplanar structures I and II with a hexagonal hole and C_1 symmetry. A close examination of these two structures finds that they correspond to a pair of enantiomers identified by the position of the hexagonal hole. The enantiomers have exactly the same electronic structures, and thus should have the same PES spectrum. Isomer III (C_s, ^{2}A″) with a hexagonal hole in the middle lies 1.90 kcal mol^{-1} above the global minima. A 3D isomer IV is found to be 3.97 kcal mol^{-1} higher, while the double ring structure V is 4.99 kcal mol^{-1} higher than the global minima. Isomer IX, which is highly non-planar with a bow-structure and a pentagonal hole, is 16.75 kcal mol^{-1} above the global minima. However, this structure is found to be the global minimum for neutral $[B_{30}]$ (Figure S2), as reported in a recent theoretical study.[28] Such divergence in global minimum structures for anions and neutrals has been observed previously for $[B_{20}]$ and $[B_{22}]$,[6,15] whose global minima were found to be planar in the anions, but the double rings in the neutral. However, no experimental evidence is available for the predicted neutral structures. A previous infrared-UV double resonance experiment on neutral boron clusters failed to detect $[B_{20}]$.[35]

To verify the anionic global minimum structures, we computed the VDEs of the low-lying isomers. The calculated VDEs of isomer I/II using the ΔSCF-TDDFT method[36] with PBE0 and TPSSh[37,38] functionals are shown with the experiment in Table 1. The VDEs from the two methods are in general consistent with each other, and we will only use the PBE0 values in the following discussion. The $[B_{30}]^-$ ion has a doublet ground state and thus both singlet and triplet neutral final states are accessible upon one-electron detachment. The first VDE refers to electron detachment from the singly occupied molecular orbital (SOMO) 46a, corresponding to the LUMO of neutral $[B_{30}]$, to produce the singlet neutral ground electronic state of the chiral isomers. The VDE of this detachment channel is calculated to be 3.72 at PBE0, in excellent agreement with the experimental VDE of band X at 3.69(7) eV. The calculated ADE of 3.60 eV at PBE0 is also in excellent agreement with the experimental ADE of 3.59(7) eV. The detachment channel from the HOMO (45a) yields the neutral triplet state, and the calculated VDE is 4.23 eV at PBE0, consistent with band A at 4.34(5) eV. The next two detachment channels have VDEs of

Table 1: The observed vertical detachment energies (VDE) for $[B_{30}]^-$ compared with the calculated values from the C_1 (^{2}A) lowest energy chiral $[B_{30}]^-$. All energies are in eV.

Feature	VDE[a] (Expt.)	Final state and electronic configuration	VDE[b] PBE0	TPSSh
X	3.69(7)	^{1}A ...38a^{2}39a^{2}40a^{2}41a^{2}42a^{2}43a^{2}44a^{2}45a^{2}46a^0	3.72	3.65
A	4.34(5)	^{3}A ...38a^{2}39a^{2}40a^{2}41a^{2}42a^{2}43a^{2}44a^{2}45a^{1}46a^1	4.23	4.07
B	4.61(5)	^{1}A ...38a^{2}39a^{2}40a^{2}41a^{2}42a^{2}43a^{2}44a^{2}45a^{1}46a^1	4.43	4.24
		^{3}A ...38a^{2}39a^{2}40a^{2}41a^{2}42a^{2}43a^{2}44a^{1}45a^{2}46a^1	4.49	4.37
C	5.03(8)	^{3}A ...38a^{2}39a^{2}40a^{2}41a^{2}42a^{2}43a^{1}44a^{2}45a^{2}46a^1	4.74	4.64
		^{1}A ...38a^{2}39a^{2}40a^{2}41a^{2}42a^{2}43a^{2}44a^{1}45a^{2}46a^1	4.80	4.63
		^{3}A ...38a^{2}39a^{2}40a^{2}41a^{2}42a^{1}43a^{2}44a^{2}45a^{2}46a^1	4.89	4.75
		^{3}A ...38a^{2}39a^{2}40a^{2}41a^{1}42a^{2}43a^{2}44a^{2}45a^{2}46a^1	4.99	4.82
		^{1}A ...38a^{2}39a^{2}40a^{2}41a^{2}42a^{2}43a^{1}44a^{2}45a^{2}46a^1	5.14	4.96
		^{1}A ...38a^{2}39a^{2}40a^{2}41a^{1}42a^{2}43a^{2}44a^{2}45a^{2}46a^1	5.23	5.17
		^{1}A ...38a^{2}39a^{2}40a^{2}41a^{2}42a^{1}43a^{2}44a^{2}45a^{2}46a^1	5.35	5.05
D	ca. 5.6	^{3}A ...38a^{2}39a^{2}40a^{1}41a^{2}42a^{2}43a^{2}44a^{2}45a^{2}46a^1	5.77	5.32
		^{1}A ...38a^{2}39a^{2}40a^{1}41a^{2}42a^{2}43a^{2}44a^{2}45a^{2}46a^1	[c]	5.49
E	ca. 5.9	^{3}A ...38a^{2}39a^{1}40a^{2}41a^{2}42a^{2}43a^{2}44a^{2}45a^{2}46a^1	5.91	5.79
F	ca. 6.2	^{3}A ...38a^{1}39a^{2}40a^{2}41a^{2}42a^{2}43a^{2}44a^{2}45a^{2}46a^1	6.51	6.44

[a] The numbers in parentheses represent the uncertainty in the last digit.
[b] Calculated at TD-DFT/6-311+G(2df)//DFT/6-311G* level of theory. [c] This value cannot be obtained at this level of theory.

4.43 eV and 4.49 eV at PBE0, which should both contribute to band B at 4.61(5) eV. Seven detachment channels are calculated to be within 4.74 eV and 5.35 eV, which are responsible for the broad band C around 5 eV. The calculated VDEs for higher detachment channels are also consistent with the experiment. The simulated spectrum of isomer I at PBE0 is shown in Figure 1b. It should be stressed that isomer II gives identical simulated spectrum.

Isomer III (C_s, $^2A''$) lies only 1.90 kcal mol^{-1} higher in energy than isomer I, and is likely to be present in the cluster beam. Its simulated spectrum is shown in Figure 1c. The calculated first VDE of isomer III is higher than that of isomer I and occurs in the X–A gap region of the PES spectrum. The non-zero intensity in the gap of bands X and A provides tentative evidence for the weak population of this isomer. We also simulated the spectra of isomers IV—VI and IX, as shown in Figure S3. Clearly, none of these agrees with the experiment. In particular, isomer IX exhibits an extremely low first VDE and its presence in the experiment can be safely ruled out. The overall good agreement between the simulated spectrum of the chiral isomer I and the experiment lends considerable credence to the obtained chiral global minimum for $[B_{30}]^-$.

To understand the chemical bonding in the chiral $[B_{30}]^-$ global minimum, we carried out adaptive natural density partitioning (AdNDP) analyses[39] for the closed-shell 2D $[B_{30}]^{2-}$ and $[B_{30}]$. The results for $[B_{30}]^{2-}$ are given in Figure S4 and those for $[B_{30}]$ are shown in Figure 3. The AdNDP

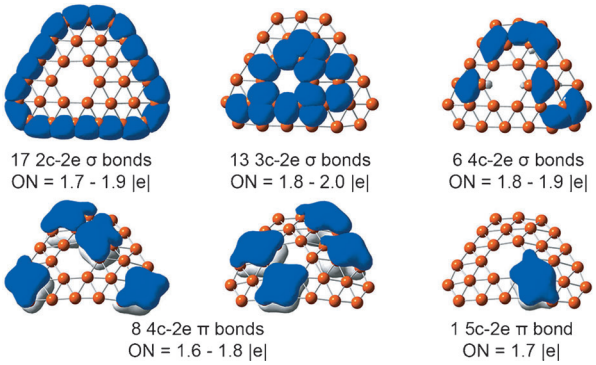

Figure 3. AdNDP chemical bonding analyses of the closed-shell $[B_{30}]$ (C_1, ^1A). ON = occupation number.

analyses of $[B_{30}]$ reveal seventeen 2c–2e σ bonds on the periphery of the quasiplanar cluster. The remaining σ electron densities are partitioned into two sets of σ delocalized bonds: thirteen 3c–2e σ bonds and six 4c–2e σ bonds. All the π electron density could be localized into eight 4c–2e and one 5c–2e π delocalized bonds, rendering π aromaticity for $[B_{30}]$ according to the (4*N*+2) Hückel rule for π electrons. Despite the aromatic character of planar $[B_{30}]$, it remains to be a high energy isomer in the neutral potential energy surface (Figure S2). Thus, we further analyzed the chemical bonding of the planar $[B_{30}]^{2-}$ by adding an electron to the global minimum of $[B_{30}]^-$. It is seen that the chemical bonding in $[B_{30}]^{2-}$ is almost identical to that in B_{30} except the additional 9c–2e π bond in $[B_{30}]^{2-}$ (Figure S4). This result reinforces the importance of delocalized π bonds in stabilizing planar boron clusters.

To understand the stability of the two enantiomers of $[B_{30}]^-$, we searched possible transition barriers between them by using the dimer method.[40] The lowest transition state is located for the inversion pathway (Figure 4), with an inversion barrier of 6.2 kcal mol^{-1} calculated at the CCSD/6-31g*

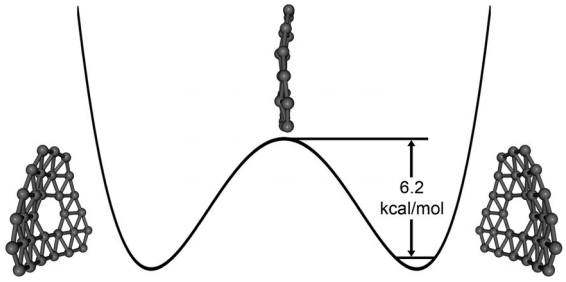

Figure 4. A schematic drawing of the potential energy curve showing the transition state between the two enantiomers of $[B_{30}]^-$ via a bending mode.

level. Vibrational analyses on the transition-state geometry show that there is only one imaginary frequency at 71*i* cm^{-1}. The barrier between the two enantiomers of $[B_{30}]^-$ is not overwhelming, and it is possible for them to convert through the out-of-plane inversion at elevated temperatures. However, when depositing the clusters onto a proper surface, such out-of-plane inversion will be inhibited, yielding two enantiomers with distinct optical activities.

In summary, we report the first inherently chiral boron cluster at $[B_{30}]^-$ using photoelectron spectroscopy and quantum chemical calculations. Excellent agreement between the calculated and experimental spectra of $[B_{30}]^-$ has confirmed the global minimum structure located by using an improved Basin-Hoping algorithm. The global minimum of $[B_{30}]^-$ is found to be a pair of 2D enantiomers characterized by different positions of the hexagonal hole. Chiral boron clusters have not been observed before, except in the boron hydride clusters $[B_4H_5]$ and $[B_4H_5]^-$ considered theoretically.[41] It is possible chiral structures may exist for larger boron clusters and such chiral clusters may be obtainable experimentally by deposition on suitable surfaces using size-selected cluster beams.

Experimental Section

Photoelectron spectroscopy: The experiment was carried out using a magnetic-bottle PES apparatus equipped with a laser vaporization cluster source, details of which can be found elsewhere.[42] Briefly, negatively charged boron clusters were produced by laser vaporization of a hot-pressed ^{10}B isotopically enriched (96%) disk target. The clusters were entrained by a He carrier gas containing 5% Ar and underwent a supersonic expansion to form a collimated and vibrationally cold cluster beam. The cluster size distribution and cooling were controlled by the time delay between the pulsed valves and the vaporization laser and the resident time of the clusters in the nozzle.[43,44] The anionic clusters were extracted from the cluster beam and analyzed with a time-of-flight mass spectrometer. The $[B_{30}]^-$

cluster was mass-selected and decelerated before being intercepted by a detachment laser beam. For the current study, the 193 nm (6.424 eV) radiation from an ArF excimer laser was used. Photoelectrons were collected at nearly 100% efficiency by a magnetic bottle and analyzed in a 3.5 m long electron flight tube. The PES spectrum was calibrated using the known spectra of Bi^- and the electron energy resolution of the apparatus was $\Delta E_k/E_k \approx 2.5\%$, that is, ca. 25 meV for 1 eV electrons.

Theoretical methods: DFT-based global-minimum searches were performed using the TGMin code developed based on an improved Basin-Hopping algorithm.[29] The calculations were carried out using the DFT formalism with the PBE[30–32] exchange-correlation functional and the Goedecker-Teter-Hutter (GTH) pseudopotential[45] with the associated double-ζ valence plus polarization (DZVP) basis set[46] for boron with the CP2K program.[47] Among more than 3600 possible structures produced by TGMin and the manually built tubular structures, we located a quasiplanar isomer with a hexagonal hole as the global minimum of $[B_{30}]^-$ (Figure 2). Its enantiomer (isomer II) is also found during the search as a distinct isomer with an identical energy. We further refined the energies by reoptimizing the geometries of low-lying isomers within 20 kcal mol^{-1} using DFT method with the hybrid PBE0 functional and the 6-311G* basis set[48–51] from the Gaussian09 program.[52] Vibrational frequencies were calculated for each isomer and all the structures were ensured to be minima on the potential energy surface without imaginary frequencies. Single-point PBE0/6-311+G(2df) calculations using Gaussian09[52] and LPNO-CCSD/def2-SVP/C[53] calculations using ORCA[54] were performed on the optimized structures obtained at the PBE0/6-311G* level of theory to get more accurate relative energies. The DLPNO-CCSD(T)[55] energies were also calculated for the low-lying isomers of the closed-shell neutral $[B_{30}]$ (Figure S2).

The PES spectra were simulated using the ΔSCF-TDDFT approach, as outlined previously.[36] Chemical bonding analyses of $[B_{30}]$ and $[B_{30}]^{2-}$ were performed using the AdNDP method.[39] All the structures are plotted using Molekel[56] and chemical bonding results are plotted using GaussView.[57]

Received: February 17, 2014
Published online: April 3, 2014

Keywords: ab initio calculations · boron clusters · borophene · chirality · photoelectron spectroscopy

[1] R. Ettl, I. Chao, F. Diederich, R. L. Whetten, *Nature* **1991**, *353*, 149–153.
[2] a) A. Lechtken, D. Schooss, J. R. Stairs, M. N. Blom, F. Furche, N. Morgner, O. Kostko, B. von Issendorff, M. M. Kappes, *Angew. Chem.* **2007**, *119*, 3002–3006; *Angew. Chem. Int. Ed.* **2007**, *46*, 2944–2948; b) I. L. Garzón, J. A. Reyes-Nava, J. I. Rodríguez-Hernández, I. Sigal, M. R. Beltrán, K. Michaelian, *Phys. Rev. B* **2002**, *66*, 073403; c) I. E. Santizo, F. Hidalgo, L. A. Perez, C. Noguez, I. L. Garzon, *J. Phys. Chem. C* **2008**, *112*, 17533–17539; d) A. J. Karttunen, M. Linnolahti, T. A. Pakkanen, P. Pyykk, *Chem. Commun.* **2008**, 465–467.
[3] T. P. Fehlner, J. F. Halet, J. Y. Saillard, *Molecular Clusters: A Bridge to Solid-State Chemitry*, Cambridge University Press, UK, **2007**.
[4] a) N. Vast, S. Baroni, G. Zerah, J. M. Besson, A. Polian, M. Grimsditch, J. C. Chervin, *Phys. Rev. Lett.* **1997**, *78*, 693–696; b) M. Fujimori, T. Nakata, T. Nakayama, E. Nishibori, K. Kimura, M. Takata, M. Sakata, *Phys. Rev. Lett.* **1999**, *82*, 4452–4455.
[5] A. Albert, H. Hillebrecht, *Angew. Chem.* **2009**, *121*, 8794–8824; *Angew. Chem. Int. Ed.* **2009**, *48*, 8640–8668.
[6] B. Kiran, S. Bulusu, H. J. Zhai, S. Yoo, X. C. Zeng, L. S. Wang, *Proc. Natl. Acad. Sci. USA* **2005**, *102*, 961–964.
[7] E. Oger, N. R. M. Crawford, R. Kelting, P. Weis, M. M. Kappes, R. Ahlrichs, *Angew. Chem.* **2007**, *119*, 8656–8659; *Angew. Chem. Int. Ed.* **2007**, *46*, 8503–8506.
[8] I. A. Popov, Z. A. Piazza, W. L. Li, L. S. Wang, A. I. Boldyrev, *J. Chem. Phys.* **2013**, *139*, 144307.
[9] H. J. Zhai, B. Kiran, J. Li, L. S. Wang, *Nat. Mater.* **2003**, *2*, 827–833.
[10] H. J. Zhai, A. N. Alexandrova, K. A. Birch, A. I. Boldyrev, L. S. Wang, *Angew. Chem.* **2003**, *115*, 6186–6190; *Angew. Chem. Int. Ed.* **2003**, *42*, 6004–6008.
[11] A. P. Sergeeva, D. Y. Zubarev, H. J. Zhai, A. I. Boldyrev, L. S. Wang, *J. Am. Chem. Soc.* **2008**, *130*, 7244–7246.
[12] W. Huang, A. P. Sergeeva, H. J. Zhai, B. B. Averkiev, L. S. Wang, A. I. Boldyrev, *Nat. Chem.* **2010**, *2*, 202–206.
[13] A. P. Sergeeva, B. B. Averkiev, H. J. Zhai, A. I. Boldyrev, L. S. Wang, *J. Chem. Phys.* **2011**, *134*, 224304.
[14] Z. A. Piazza, W. L. Li, C. Romanescu, A. P. Sergeeva, L. S. Wang, A. I. Boldyrev, *J. Chem. Phys.* **2012**, *136*, 104310.
[15] A. P. Sergeeva, Z. A. Piazza, C. Romanescu, W. L. Li, A. I. Boldyrev, L. S. Wang, *J. Am. Chem. Soc.* **2012**, *134*, 18065–18073.
[16] I. Boustani, A. Quandt, E. Hernandez, A. Rubio, *J. Chem. Phys.* **1999**, *110*, 3176–3185.
[17] M. H. Evans, J. D. Joannopoulos, S. T. Pantelides, *Phys. Rev. B* **2005**, *72*, 045434.
[18] J. Kunstmann, A. Quandt, *Phys. Rev. B* **2006**, *74*, 035413.
[19] I. Cabria, J. A. Alonso, M. J. López, *Phys. Status Solidi A* **2006**, *203*, 1105–1110.
[20] I. Cabria, M. J. López, J. A. Alonso, *Nanotechnology* **2006**, *17*, 778–785.
[21] K. C. Lau, R. Pandey, *J. Phys. Chem. C* **2007**, *111*, 2906–2912.
[22] H. Tang, S. Ismail-Beigi, *Phys. Rev. Lett.* **2007**, *99*, 115501.
[23] X. B. Yang, Y. Ding, J. Ni, *Phys. Rev. B* **2008**, *77*, 041402R.
[24] L. A. Chernozatonskii, P. B. Sorokin, B. I. Yakobson, *JETP Lett.* **2008**, *87*, 489–493.
[25] Y. Ding, X. Yang, J. Ni, *Appl. Phys. Lett.* **2008**, *93*, 043107.
[26] H. Tang, S. Ismail-Beigi, *Phys. Rev. B* **2010**, *82*, 115412.
[27] Z. A. Piazza, H. S. Hu, W. L. Li, Y. F. Zhao, J. Li, L. S. Wang, *Nat. Commun.* **2014**, DOI: 10.1038/ncomms4113.
[28] T. B. Tai, L. V. Duong, H. T. Pham, D. T. T. Mai, M. T. Nguyen, *Chem. Commun.* **2014**, *50*, 1558–1560.
[29] Y. F. Zhao, J. Li, *Nano Res.*, in press.
[30] C. Adamo, V. Barone, *J. Chem. Phys.* **1999**, *110*, 6158–6170.
[31] J. P. Perdew, K. Burke, M. Ernzerhof, *Phys. Rev. Lett.* **1996**, *77*, 3865–3868.
[32] J. P. Perdew, K. Burke, M. Ernzerhof, *Phys. Rev. Lett.* **1997**, *78*, 1396–1396.
[33] F. Neese, F. Wennmohs, A. Hansen, *J. Chem. Phys.* **2009**, *130*, 114108.
[34] F. Neese, A. Hansen, D. G. Liakos, *J. Chem. Phys.* **2009**, *131*, 064103.
[35] C. Romanescu, D. J. Harding, A. Fielicke, L. S. Wang, *J. Chem. Phys.* **2012**, *137*, 014317.
[36] a) J. Li, X. Li, H. J. Zhai, L. S. Wang, *Science* **2003**, *299*, 864–867; b) B. Kiran, X. Li, H. J. Zhai, L. F. Cui, L. S. Wang, *Angew. Chem.* **2004**, *116*, 2177–2181; *Angew. Chem. Int. Ed.* **2004**, *43*, 2125–2129.
[37] V. N. Staroverov, G. E. Scuseria, J. M. Tao, J. P. Perdew, *J. Chem. Phys.* **2003**, *119*, 12129–12137.
[38] J. Tao, J. P. Perdew, V. N. Staroverov, G. E. Scuseria, *Phys. Rev. Lett.* **2003**, *91*, 146401.
[39] D. Y. Zubarev, A. I. Boldyrev, *Phys. Chem. Chem. Phys.* **2008**, *10*, 5207–5217.
[40] G. Henkelman, H. Jónsson, *J. Chem. Phys.* **1999**, *111*, 7010–7022.
[41] J. K. Olson, A. I. Boldyrev, *Chem. Phys. Lett.* **2011**, *517*, 62–67.

[42] L. S. Wang, H. S. Cheng, J. W. Fan, *J. Chem. Phys.* **1995**, *102*, 9480 – 9493.
[43] W. Huang, L. S. Wang, *Phys. Rev. Lett.* **2009**, *102*, 153401.
[44] J. Akola, M. Manninen, H. Häkkinen, U. Landman, X. Li, L. S. Wang, *Phys. Rev. B* **1999**, *60*, 11297 – 11300.
[45] S. Goedecker, M. Teter, J. Hutter, *Phys. Rev. B* **1996**, *54*, 1703 – 1710.
[46] J. VandeVondele, J. Hutter, *J. Chem. Phys.* **2007**, *127*, 114105.
[47] J. VandeVondele, M. Krack, F. Mohamed, M. Parrinello, T. Chassaing, J. Hutter, *Comput. Phys. Commun.* **2005**, *167*, 103 – 128.
[48] R. Krishnan, J. S. Binkley, R. Seeger, J. A. Pople, *J. Chem. Phys.* **1980**, *72*, 650 – 654.
[49] M. S. Gordon, J. S. Binkley, J. A. Pople, W. J. Pietro, W. J. Hehre, *J. Am. Chem. Soc.* **1982**, *104*, 2797 – 2803.
[50] W. J. Pietro, M. M. Francl, W. J. Hehre, D. J. Defrees, J. A. Pople, J. S. Binkley, *J. Am. Chem. Soc.* **1982**, *104*, 5039 – 5048.
[51] T. Clark, J. Chandrasekhar, G. W. Spitznagel, P. V. Schleyer, *J. Comput. Chem.* **1983**, *4*, 294 – 301.
[52] M. J. Frisch, et al., Gaussian, Inc., Wallingford CT, **2009**.
[53] F. Weigend, R. Ahlrichs, *Phys. Chem. Chem. Phys.* **2005**, *7*, 3297 – 3305.
[54] The ORCA program system: F. Neese, *WIREs Comput. Mol. Sci.* **2012**, *2*, 73 – 78.
[55] F. Neese, C. Riplinger, *J. Chem. Phys.* **2013**, *138*, 034106.
[56] U. Varetto, Molekel 5.4.0.8, Swiss National Supercomputing Centre, Manno, Switzerland, **2009**.
[57] R. Dennington, Todd Keith, J. Millam, Semichem, Inc., Shawnee Mission, KS, 2007, **2007**.

